NANO LETTERS

pubs.acs.org/NanoLett

Letter

Varifocal Metalens for Optical Sectioning Fluorescence Microscopy

Yuan Luo,*,† Cheng Hung Chu,† Sunil Vyas,† Hsin Yu Kuo,† Yu Hsin Chia, Mu Ku Chen, Xu Shi, Takuo Tanaka, Hiroaki Misawa, Yi-You Huang, and Din Ping Tsai*

Cite This: *Nano Lett.* 2021, 21, 5133−5142

Read Online

ACCESS | Metrics & More | Article Recommendations | Supporting Information

ABSTRACT: Fluorescence microscopy with optical sectioning capabilities is extensively utilized in biological research to obtain three-dimensional structural images of volumetric samples. Tunable lenses have been applied in microscopy for axial scanning to acquire multiplane images. However, images acquired by conventional tunable lenses suffer from spherical aberration and distortions. Here, we design, fabricate, and implement a dielectric Moiré metalens for fluorescence imaging. The Moiré metalens consists of two complementary phase metasurfaces, with variable focal length, ranging from ∼10 to ∼125 mm at 532 nm by tuning mutual angles. In addition, a telecentric configuration using the Moiré metalens is designed for high-contrast multiplane fluorescence imaging. The performance of our system is evaluated by optically sectioned images obtained from HiLo illumination of fluorescently labeled beads, as well as ex vivo mice intestine tissue samples. The compact design of the varifocal metalens may find important applications in fluorescence microscopy and endoscopy for clinical purposes.

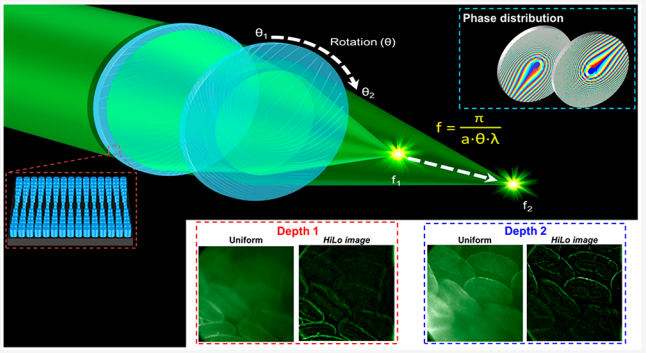

KEYWORDS: *metasurface, fluorescence microscopy, optical sectioning, telecentric configuration, HiLo imaging*

Wide-field fluorescence microscopy is a fundamental technique to investigate structural details of biological specimens for various imaging applications.[1−3] However, wide-field microscopy suffers from poor image contrast because out-of-focus background noise degrades image quality. Various optical sectioning methods have been introduced to obtain three-dimensional fluorescence images with high-contrast.[4−7] Among optical sectioning microscopes, confocal microscopy[8,9] is the most commonly utilized but has limitation of point-by-point scanning.[10] Alternative techniques to the confocal microscopy, optical sectioning capability can be achieved computationally using structured illumination imaging.[4,11,12] A simple and effective way to achieve fine optical sectioning capability in wide-field detection is through HiLo imaging.[13−15] HiLo microscopy is a structured illumination technique where optically sectioned images are computationally acquired from pairwise images.[16−18] Although HiLo microscopy can provide high contrast multiplane images, it still requires scanning samples in the axial direction. However, maintaining high contrast up to long scanning range is not straightforward. A tunable lens in microscopy provides remote focusing to avoid shift disturbance and increase axial scanning speed.[19] In general, to maintain constant magnification in optical systems, axial displacements of conventional zoom lenses have been used. Miniaturization of zoom lenses is difficult because of the requirement of complicated wavefront compensation to reduce aberrations. Based on different physical mechanisms, a few tunable focal lenses (TFLs) have been proposed.[20,21] Most recently used TFLs include liquid crystal and elastomeric membrane lenses. The former has limitations of nonimmediate response, spherical aberration, and distortion from nonideal spherical profiles.[22] The latter has not only the above-described limitations but also can be barely used in a vertical direction due to gravity effects. Dynamic devices, such as spatial light modulators (SLMs) and deformable mirrors, are bulky, and their pixelated structures result in low resolution and unwanted diffraction orders.

Bernet et al. proposed a Moiré lens composed of two paired phase plates with complementary phase profiles.[23−25] The combined phase of the two plates is equivalent to a focusing lens, the focal length of which can be adjusted by tuning mutual angles rather than lateral or axial shift. Traditional optics shape the light wavefront by phase accumulation in the propagation path, which inevitably leads to thick optical components and bulky optical systems. In recent years, many efforts have been made to miniaturize optical modules with

Received: March 18, 2021
Revised: May 18, 2021
Published: June 7, 2021

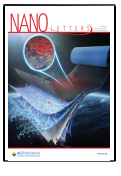

https://doi.org/10.1021/acs.nanolett.1c01114
Nano Lett. 2021, 21, 5133−5142

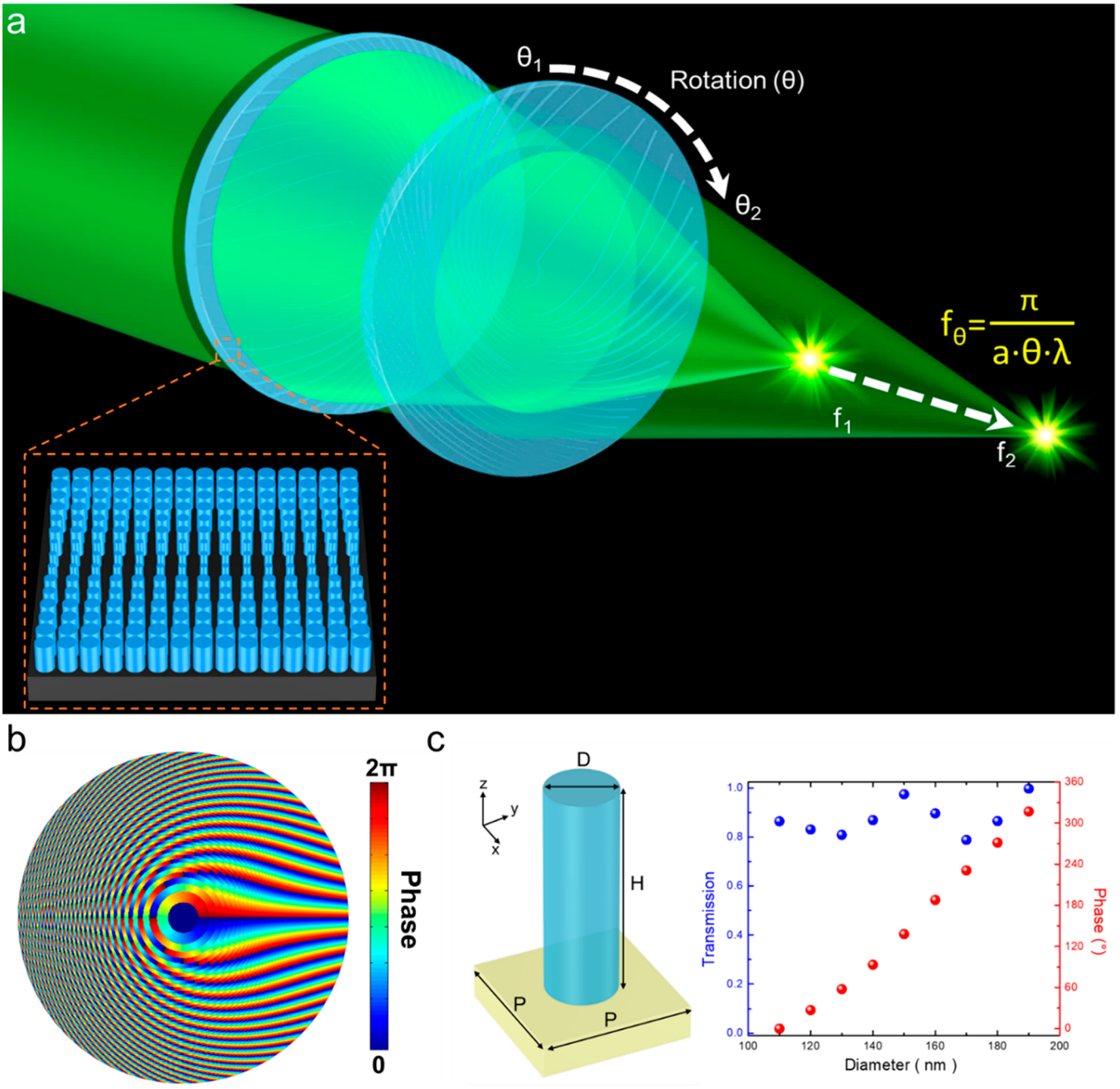

Figure 1. Design principle of variable focus Moiré metalens. (a) Schematic diagram of the Moiré metalens. The focal length (f_θ) can be adjusted by changing relative angles of the paired metasurfaces. (b) Designed phase distribution of a metasurface for the varifocal lens. (c) Unit cell consisting of GaN nanopillars with a height of 800 nm (H) and a period of 250 nm (P) on a sapphire substrate. The corresponding transmission and phase shift of GaN nanopillars with different diameters.

diffractive optics and computational methods to optimize their performance by novel fabrication processes to directly reduce the size of optical components.[26,27] However, the fabrication of miniature optical elements with curved surfaces with sophisticated phase distribution and their integration with optical systems are still challenging. Metasurfaces are emerging techniques and have attracted many interests because of their exceptional abilities to create various optical components on demand, such as lenses,[28,29] polarization optical components,[30] holograms,[31] and spectral filters.[32] The ability to manipulate optical properties at the nanoscale, such optical elements are suitable for materials applications, including quantum state generation,[33] biomedical imaging or sensing,[34,35] and light field imaging.[36,37] The realization of nanophotonic components relies on the engineering phase, amplitude, and polarization of electromagnetic waves by using the optical resonance of subwavelength structures.[38] Low-loss high-refractive-index dielectric materials are commonly used to improve the efficiency of metasurfaces. Recently, near or middle infrared varifocal metalens has been implemented by using the Alvarez method,[39,40] MEMS system,[41] Moiré effect,[42,43] and stretchable material.[44]

In this work, we introduce a dielectric Moiré metalens, which is composed of two complementary flat GaN metasurface phase plates, to perform fluorescence bioimaging applications in visible regions. Because of its natural material

https://doi.org/10.1021/acs.nanolett.1c01114
Nano Lett. 2021, 21, 5133−5142

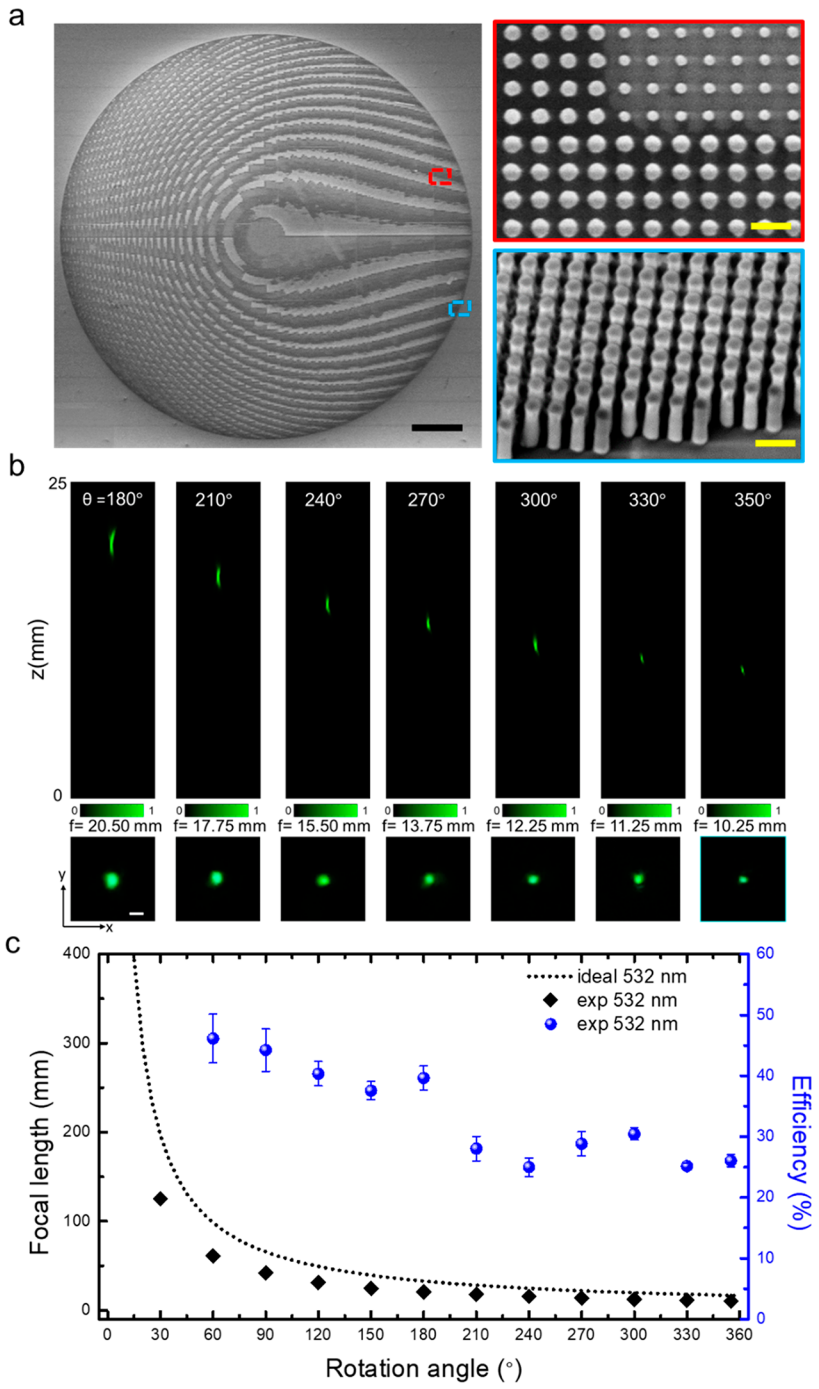

Figure 2. Optical characteristics of the Moiré metalens. (a) Scanning electron microscope (SEM) images of the fabricated metasurface with diameter of 1.6 mm. Scale bar: 200 μm. Top-view (red square) and tiled-view (blue square) zoomed-in SEM image of unit cells of the metasurface. Scale bar: 1 μm. (b) Experimentally measured focusing behavior of the Moiré metalens and corresponding focal spots (bottom images) at different relative rotation angles (θ = 180−350°) of the paired metasurfaces at λ = 532 nm. Scale bar: 100 μm. (c) Experimental and theoretical focal length and measured efficiency of Moiré metalens (at λ = 532 nm) at different relative rotation angles (θ = 30−350°).

characteristics of low loss and high refractive index in visible spectrum,[45,46] GaN is suitable for fabricating metalens. Different diameters of cylindrical nanopillars are used to construct a Moiré metalens to provide a full 2π phase requirement without polarization dependence. The focal length of our metalens can be tuned from ∼10 mm to ∼125 mm with an average efficiency of ∼40% at a wavelength of 532 nm by changing the mutual angles between two phase plates. In addition, we experimentally demonstrate optically sectioned multiplane images of ex vivo mice villi tissue samples through HiLo microscopy, based on telecentric design, as well as the variable focus metalens. To the best of our knowledge, this is the first report on applications of the variable focus metalens for optical sectioning fluorescence microscopy. The wide range of tunability with constant magnification offered by our method will help in multiplane bioimaging of various biological samples.

https://doi.org/10.1021/acs.nanolett.1c01114
Nano Lett. 2021, 21, 5133−5142

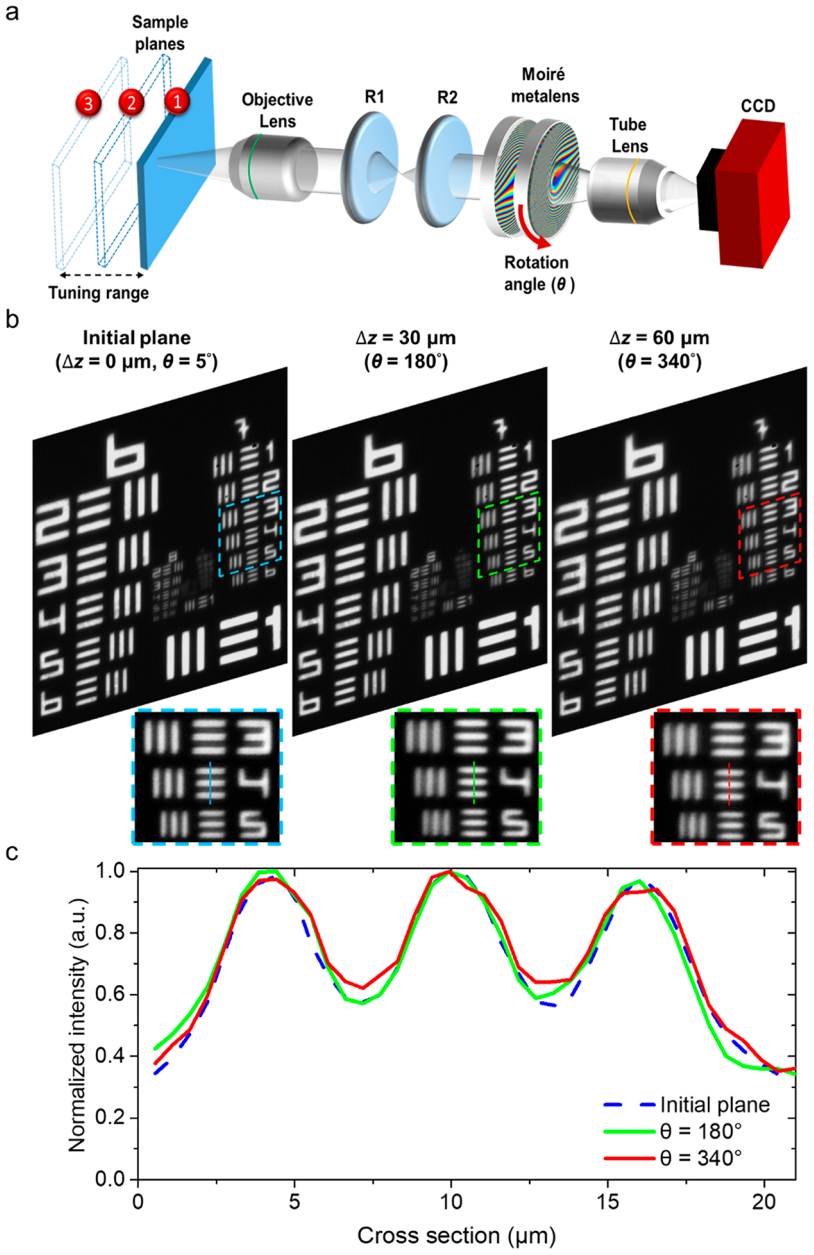

Figure 3. Invariant magnification images in the Moiré metalens based microscope, with telecentric design. (a) Experimental setup for invariant magnification imaging during focus adjustment. In the telecentric setup, our Moiré metalens is positioned at the Fourier plane of the objective to obtain uniform magnification and contrast images. (b) Three in-focus images of the 1951 United States Air Force resolution chart at different focal planes (Δz = 0, 30, and 60 μm) by adjusting relative angles of the Moiré metalens. (c) Normalized intensity of cross sections along the dashed lines at Δz = 0 μm (left), Δz = 30 μm (middle), and Δz = 60 μm (right), respectively. The MTF, which is defined as $(I_{max} - I_{min})/(I_{max} + I_{min})$, of blue, green, and red curves are 0.28, 0.28, and 0.23, respectively. I_{max} (I_{min}) is the maximum (minimum) intensity along the cross-section profiles.

RESULTS AND DISCUSSION

A schematic of the Moiré metalens, which is composed of a pair of planar metasurfaces, is illustrated in Figure 1a. The focal length of the Moiré metalens can be adjusted by changing relative angles between paired metasurfaces. Phase distribution of the metasurfaces is designed by the principle of the Moiré lens method.[47] GaN nanopillars with different diameters are arranged on a sapphire surface to satisfy phase requirements. On the basis of the Moiré lens method, two identical metasurfaces are designed and placed face to face such that one is upside down with respect to other.[47] The phase distribution of the metasurface is shown in Figure 1b according to the following equation:

$$\Phi(r, \theta_0) = \text{round}\left(\frac{1}{\lambda \cdot F_0} r^2\right)\theta_0 \quad (1)$$

where λ is the operation wavelength, F_0 represents the reference focal length, r is the radial coordinate on metasurface, and θ_0 denotes the reference rotation angle. The round(•) function transforms the value of the operand to the nearest integer to avoid the sectoring effect.[47] The phase modulated light passing through the paired metasurfaces can be described as

$$\Phi_{integral} = \Phi(r, \theta_0) + (-\Phi(r, \theta_0 - \theta)) = ar^2\theta \quad (2)$$

https://doi.org/10.1021/acs.nanolett.1c01114
Nano Lett. 2021, 21, 5133−5142

where a is a constant and θ denotes the relative angle between the paired metasurfaces. To realize the phase requirement of the focus lens, a can be adopted as $1/\lambda F_0$. Here, we set $a = 100$ mm^{-2}. The relationship between the tunable focal length (f_θ) and relative angle (θ) can be written as

$$f_\theta = \pi/a\theta\lambda \tag{3}$$

In Figure 1c, the height of GaN nanopillars and period of each unit cell are 800 and 250 nm, respectively. Different diameters (D) of GaN nanopillars, ranging from 110 to 190 nm, can provide various distinct phase shifts and high transmission up to 80% (detailed information about the simulation can be found in Supporting Information Section 1).

We utilized electron beam lithography (EBL), plasma-enhanced chemical vapor deposition (PECVD), and inductively coupled-plasma reactive ion etching (ICP-RIE) to fabricate the metasurfaces[46] (the detailed information is discussed in Methods). The SEM images of fabricated metasurface are shown in Figure 2a. The diameter of metasurface is 1.6 mm. We experimentally demonstrated the performance of the Moiré metalens with different relative angles between the paired metasurfaces at a wavelength of 532 nm (see Figure S2 for description of the measurement setup). Figure 2b shows the measured focus beam profiles of the Moiré metalens along the propagation direction under different rotation angles (θ = 180−350°) in a step of 30°. The focal length is a function of rotation angle (θ) and decreases with the increasing relative rotation angles of the metasurfaces. The shape of point spread function appears elongated ellipsoids in $x-z$ plane. In Figure 2c, the focal lengths are shown as a function of the rotation angles which is in qualitative agreement with theoretical predictions. The tunable focus range of our metalens can be adjusted from 10 to 125 mm at λ = 532 nm. The average focusing efficiency of our Moiré metalens, which is defined as a ratio between the incident optical power of the focal spot area and that of the incident light source, is around 35% at the wavelength of 532 nm. Furthermore, we have measured the focusing behavior of the Moiré metalens at λ = 633 and 491 nm, respectively (see Figure S2). The tunable focal length property is demonstrated by focal intensity measurements, and the negative dispersion property (in supplementary, the focal length of red light is shorter than that of blue light) in point spread function in the visible spectrum is also observed. Because the Moiré lens is a cascaded optical system that inevitably suffers from misalignment in assembling, the alignment tolerance has to be taken into account. The deformation of transmission function of a Moiré lens under different degrees of lateral misalignment is studied previously.[23] It is demonstrated that two phase plates with 2% decentration without a high pixel-to-pixel matching level still can maintain focusing functionality with reasonable accuracies. Further, the point spread function of Moiré lens splits under large misalignment.[47] To quantify the influence of misalignment for our system, we image a standard 1951 United States Air Force (USAF) resolution chart under different lateral shifts of two phase plates (in Figure S4). Indeed, the slight misalignment leads to image distortion, but it does not destroy the imaging functionality. Modulation transfer function (MTF) of a misaligned system is also evaluated. The misalignment tolerance of approximately 70 μm, 4.4% of the metalens diameter, is demonstrated and acceptable for practical application.

Telecentric design is an important technique for image-based optical metrology because of its advantages of parallax error-free imaging.[48] To obtain high-quality images of biological samples, uniform magnification and illumination are essential. The direct benefit of telecentric configuration in the microscope system is that it provides an extended axial scanning range with uniform magnification and image contrast throughout the focal depth.[19,49] Figure 3 shows our designed Moiré metalens-based microscope in a telecentric configuration. As shown in Figure 3a, the transmitted light is collected by an objective (Mitutoyo, BD Plan Apo 20×, NA = 0.42) and passes through a 4f relay lens set up. The Moiré metalens is located at the Fourier plane of the front objective lens to adjust the focal length in the system. Resultant images with uniform magnification and contrast are collected by a tube lens (Mitutoyo, BD Plan Apo 5× , NA = 0.14), and projected onto a charge coupled device (CCD, Prosilica GE1650). The shifted distance at the object plane in the telecentric design through the Moiré metalens can be written as

$$\Delta z = \frac{n}{M^2}\frac{f_r^2}{f_\theta} \tag{4}$$

where n denotes refractive index of the sample space, M is the effective magnification of the front objective lens and first relay lens (R1) (Thorlabs, Achromatic Doublet, f = 100 mm), f_r represents the equivalent focal length of the second relay lens (R2), and (f_θ) is the tunable focal length of our Moiré metalens. As Moiré metalens is located at the Fourier plane, the combination of the R2 and Moiré metalens can be considered as a compound lens, whose focal length is equivalent to the focal length of the relay lens (R2).[19] According to eq 3, the scanning range at the object plane can be described as

$$\Delta s = \Delta z_{max} - \Delta z_{min} = \frac{n}{M^2}\frac{f_r^2 a\lambda}{\pi}(\theta_{max} - \theta_{min}) \tag{5}$$

The relationship between scanning range (Δs) and relative rotation angle ($\Delta\theta$) is linear. A USAF resolution target resolution chart is imaged with a green laser light source (λ = 532 nm) to test the imaging performance of the Moiré metalens based microscope. The smallest features of 2.19 μm at group 7 element 6 on the resolution target are well observed in Figure 3. In this experiment, the displacement of focal plane is linearly proportional to the rotation angle of the Moiré metalens. To check constant magnification of the system during the entire axial scanning, the same region of interest are compared in Figure 3b, which also show zoomed-in in-focus images of the USAF resolution target (elements 3−5 of group 7) at different depths from Δz = 0 μm to Δz = 60 μm (corresponding to rotation angles from 5 to 340°). (More detailed information on the scanning process can be found in the Supporting Information). The normalized intensity profiles of element 4 are plotted in Figure 3c, which demonstrates that the image quality (both magnification and contrast) of our imaging system remains constant during axial scanning.

We applied the HiLo imaging process to acquire optically sectioned images in our experiments. An optically sectioned image i_{os} is obtained for both in-focus Hi and Lo images, as follows:

$$i_{os} = \mathrm{Hi}(x, y) + \eta \mathrm{Lo}(x, y) \tag{6}$$

https://doi.org/10.1021/acs.nanolett.1c01114
Nano Lett. 2021, 21, 5133−5142

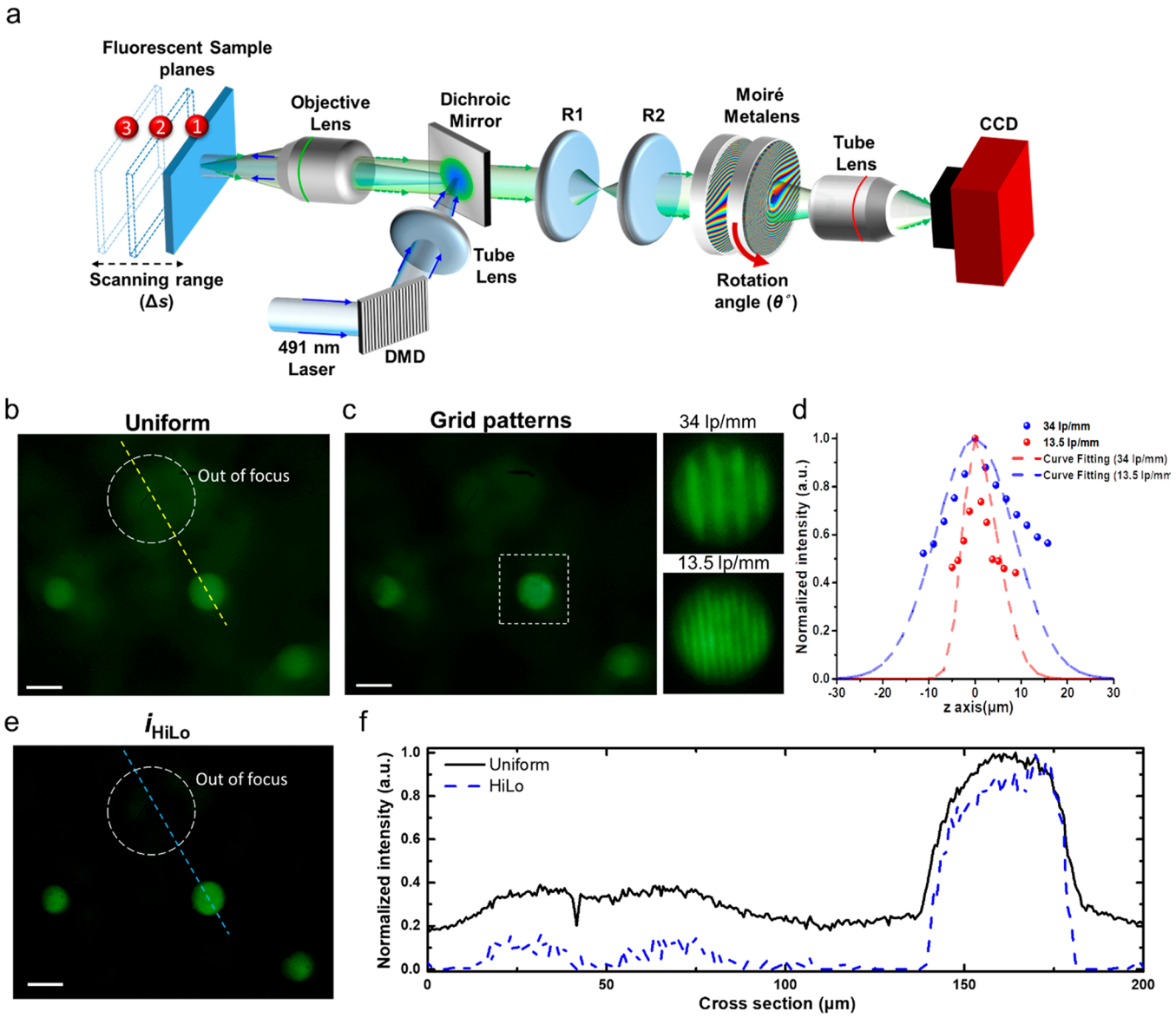

Figure 4. Fluorescent images of microspheres using Moiré metalens based microscopy with the HiLo principle. (a) Experimental setup of the epi-illumination fluorescence microscope based on a telecentric design with variable focus Moiré metalens. The fluorescent images of 45 μm microspheres, under (b) uniform illumination and (c) structured illumination. Scale bar: 45 μm. The insets show the zoomed-in images of a fluorescent microsphere using grid patterns with 34 lp/mm (top) and 13.5 lp/mm (bottom). (d) Optical sectioning capability of the microscope for two grid patterns with 34 lp/mm (marked with red color) and 13.5 lp/mm (marked with blue color). (e) HiLo processed image of fluorescent microspheres obtained by structured illumination using the grid pattern with 34 lp/mm. Scale bar: 45 μm. (f) Comparison of intensity profiles along dashed lines between uniform (b) and HiLo images (e).

where η is the scaling constant to combine Hi and Lo images. The typical value of η in our experiment is in the range of 0.6–1.5. (The details of the HiLo imaging process are discussed in Supporting Information Section 6.)

An epi-illumination fluorescence microscope based on telecentric design and Moiré metalens is built, as shown in Figure 4a. The Moiré metalens is positioned at the Fourier plane, and structured illumination is generated through a digital mirror device (DMD). The fluorescent microspheres (Fluoresbrite YG microspheres 45 μm in diameter, Polysciences) are excited using a blue laser source at λ = 491 nm (CalypsoTM, Cobalt Inc.) under uniform and structured illumination (the grid patterns with different spatial frequencies of 34 lp/mm and 13.5 lp/mm produced by the DMD), respectively, as shown in Figure 4b. The projected grid patterns are well observed at the in-focus microspheres, as shown in Figure 4c. The experimentally measured optical sectioning capability of our microscope under structured illumination is shown in Figure 4d. The full width at half-maximum (fwhm) of optical sectioning capability is respective ~7.5 and 29.25 μm for two grid patterns with corresponding spatial frequencies of 34 lp/mm and 13.5 lp/mm. It is noticed that higher spatial frequency provides finer optical sectioning capability. Figure 4e shows the optically sectioned fluorescent image, obtained by the HiLo principle using the grid pattern with the spatial frequency of 34 lp/mm. Figure 4f shows the comparison of intensity profiles along dashed lines between uniform (i.e., wide-field) and HiLo processed images. In the HiLo imaging process, the out-of-focus background noise is

https://doi.org/10.1021/acs.nanolett.1c01114
Nano Lett. 2021, 21, 5133−5142

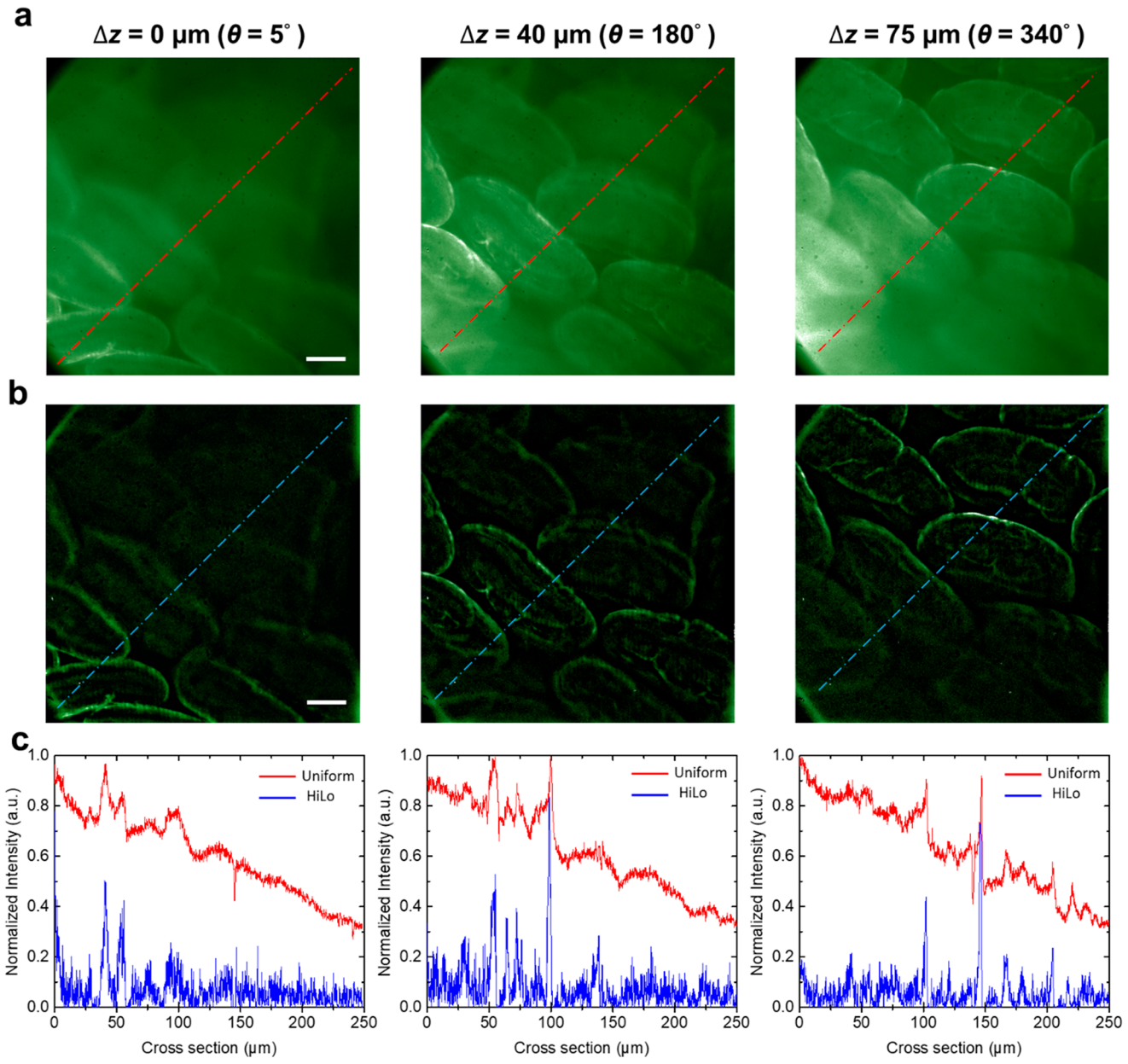

Figure 5. Ex vivo images of intestine tissue samples at different depths. (a) Fluorescent images of villi under uniform illumination at three different depths (Δz = 0 μm, Δz = 40 μm, and Δz = 75 μm) are obtained by rotating the relative angles between metasurfaces. (b) HiLo processed images of villi at three corresponding depths. Scale bar: 25 μm. (c) Intensity cross sections along dashed lines in uniform illuminated images (red line) and HiLo processed images (blue line) with Δz = 0, 40, and 75 μm, respectively.

suppressed significantly, and the in-focus optical sectioning images of microspheres are clearly observed.

The performance of our Moiré metalens based microscope to resolve volumetric samples is evaluated by imaging fluorescently labeled mice intestine tissue samples (the detailed process of fluorescent dyeing is discussed in Supporting Information Section 7). The ex vivo images of villi of the intestine sample under uniform illumination at three different depths are shown in Figure 5a. Three different focal depths are obtained by changing rotation angles of Moiré metalens from 5 to 340°, with the maximum tunable focus range of around 75 μm. Haze is significantly visible because of the nature of the thick sample under uniform illumination. Figure 5b shows the significant removal of the haze, and optically sectioned images of villi are obtained through the HiLo imaging process. The out-of-focus background noise is significantly suppressed, while in-focus fine structures of villi are clearly observed (ex vivo images of villi under structured illumination can be further found in Figure S7). To quantitatively analyze, we measured the intensity cross sections of uniformly illuminated and HiLo processed images at different depths, as shown in Figure 5c. The detailed structures in the resultant images are obtained with a good signal-to-background ratio.

CONCLUSIONS

In conclusion, following the Moiré technique, a variable focus dielectric metalens is designed and implemented for high-contrast optical sectioning fluorescence microscopy at the visible spectral region. The design principle of the Moiré metalens and telecentric design are described in detail. We

https://doi.org/10.1021/acs.nanolett.1c01114
Nano Lett. 2021, 21, 5133−5142

demonstrated telecentric imaging equipped with variable focus metalens, which performs high-contrast multiplane fluorescence imaging for ex vivo mice intestine tissue samples. In addition, Moiré metalens-based fluorescence microscopy with the HiLo imaging principle provides fine optical sectioning with invariant image contrast through the entire scanning range. The scanning range of the Moiré metalens based microscope is ∼75 μm, which can be further extended with low NA objectives. The long tuning range with constant magnification obtained from our system will be advantageous in obtaining high-contrast multiplane images for biomedical research. As a clear demonstration of imaging performance for our Moiré metalens-based microscope, both standard resolution target and fluorescent microspheres are imaged, with a lateral resolution of ∼2 μm, as well as optical sectioning capability of ∼7 μm. The varifocal Moiré metalens with ultrathin size and compact design may replace its counterpart in any optical system that requires a focus-tunable lens, such as optical coherence tomography[50] and microendoscopy[19] for in vivo imaging.

METHODS

Fabrication of the GaN Metalens. The 800 nm c-plane GaN thin film is grown on a double-polished c-plane sapphire substrate by metalorganic chemical vapor deposition (MOCVD), and the 400 nm SiO_2 thin film is deposited by PECVD on it as hard mask layer. The photoresist, diluted ZEP-520A (ZEP-520A:ZEPA = 1:1), is spin-coated (thickness ∼150 nm) onto the substrate. The nanostructure pattern is defined by an electron beam lithography system (Elionix ELS-7000). After development, the 35 nm Cr thin film as hard mask layer is deposited on the sample by an electron-gun evaporator. N,N-Dimethylacetamide (ZDMAC) solution is used to remove the residual photoresist on the surface in the lift-off process. The designed nanostructure patterns are formed onto a 400 nm SiO_2 hard mask layer by reactive ion etching using CHF_3 gas with 90 W plasma power. Subsequently, the GaN layer is etched by ICP-RIE with BCl_3/Cl_2 chemistry in 700 W ICP source power and 280 W bias power. Last, the GaN metasurface for the Moiré metalens is completed after removing the residual SiO_2 hard mask by a buffered oxide etch solution.

ASSOCIATED CONTENT

Supporting Information

The Supporting Information is available free of charge at https://pubs.acs.org/doi/10.1021/acs.nanolett.1c01114.

Detailed discussion of the sample fabrication, experimental detail, and discussion; nanofabrication processes of metasurfaces; focus behavior of varifocal Moiré metalens; misalignment tolerance of varifocal Moiré metalens; investigation of focus displacement and invariant system magnification; derivation of HiLo imaging process; fluorescent dyeing process for tissue sample preparation; ex vivo images of villi under structured illumination for HiLo process (PDF)

AUTHOR INFORMATION

Corresponding Authors

Din Ping Tsai − *Research Center for Applied Sciences, Academia Sinica, Taipei 11529, Taiwan; Department of Physics, National Taiwan University, Taipei 10617, Taiwan; Department of Electronic and Information Engineering, The Hong Kong Polytechnic University, Kowloon 999077, Hong Kong;* orcid.org/0000-0002-0883-9906; Email: dinping.tsai@polyu.edu.hk

Yuan Luo − *Institute of Medical Device and Imaging and Institute of Biomedical Engineering, National Taiwan University, Taipei 10051, Taiwan; YongLin Institute of Health, National Taiwan University, Taipei 10672, Taiwan;* Email: yuanluo@ntu.edu.tw

Authors

Cheng Hung Chu − *Institute of Medical Device and Imaging, National Taiwan University, Taipei 10051, Taiwan; Research Center for Applied Sciences, Academia Sinica, Taipei 11529, Taiwan; Innovative Photon Manipulation Research Team, RIKEN Center for Advanced Photonics, Saitama 351-0198, Japan*

Sunil Vyas − *Institute of Medical Device and Imaging, National Taiwan University, Taipei 10051, Taiwan*

Hsin Yu Kuo − *Institute of Medical Device and Imaging, National Taiwan University, Taipei 10051, Taiwan; Research Center for Applied Sciences, Academia Sinica, Taipei 11529, Taiwan; Department of Physics, National Taiwan University, Taipei 10617, Taiwan*

Yu Hsin Chia − *Institute of Medical Device and Imaging and Institute of Biomedical Engineering, National Taiwan University, Taipei 10051, Taiwan*

Mu Ku Chen − *Department of Electronic and Information Engineering, The Hong Kong Polytechnic University, Kowloon 999077, Hong Kong;* orcid.org/0000-0002-6697-0398

Xu Shi − *Research Institute for Electronic Science Hokkaido University, Sapporo 001-0021, Japan;* orcid.org/0000-0002-6353-5470

Takuo Tanaka − *Innovative Photon Manipulation Research Team, RIKEN Center for Advanced Photonics, Saitama 351-0198, Japan; Metamaterial Laboratory, RIKEN Cluster for Pioneering Research, Saitama 351-0198, Japan; Institute of Post-LED Photonics, Tokushima University, Tokushima 770-8506, Japan;* orcid.org/0000-0001-5714-5401

Hiroaki Misawa − *Research Institute for Electronic Science Hokkaido University, Sapporo 001-0021, Japan;* orcid.org/0000-0003-1070-387X

Yi-You Huang − *Institute of Biomedical Engineering, National Taiwan University, Taipei 10051, Taiwan; Department of Biomedical Engineering, National Taiwan University Hospital, Taipei 100225, Taiwan*

Complete contact information is available at: https://pubs.acs.org/10.1021/acs.nanolett.1c01114

Author Contributions

C.H.C., S.V., and H.Y.K. performed the numerical simulation and metasurface design, performed the characterization of the metasurface, and built up the optical system to perform all the measurements. C.H.C., M.K.C., X.S., T.T., and H.M. helped in fabrication of the metasurface. Y.H.C. prepared mouse heart tissues. C.H.C., S.V., H.Y.K., Y.L., Y.Y.H., M.K.C, and D.P.T. cowrote the manuscript. Y.L., Y.Y.H., and D.P.T. supervised this work. Y.L., Y.Y.H., and D.P.T. organized the project, analyzed the results, and prepared the manuscript. All authors discussed the results and commented on the manuscript.

Author Contributions

†Y.L. C.H.C., S.V., and H.Y.K. contributed equally to this work.

Notes

The authors declare no competing financial interest.

https://doi.org/10.1021/acs.nanolett.1c01114
Nano Lett. 2021, 21, 5133−5142

■ ACKNOWLEDGMENTS

C.H.C., S.V., H.Y.K., Y.L., and Y.Y.H. acknowledge support from Ministry of Science and Technology, Taiwan (Grants MOST- 106-2221-E-002-157-MY3, MOST-108-2221-E-002-168-MY4, MOST-109-2221-E-002-048) and National Taiwan University (Grant NTU-YIH-08HZT49001). C.H.C. and T.T. acknowledge support from Core Research for Evolutional Science and Technology of Japan Science and Technology Agency (Grant JPMJCR1904). X.S. and H.M. acknowledge support from Grants-in-Aid for Scientific Research of Japan Society for the Promotion of Science (Grant JP18H05205). M.K.C, and D.P.T. acknowledge support from Shenzhen Science and Technology Innovation Commission (Grant SGDX2019081623281169), University Grants Committee/Research Grants Council of the Hong Kong Special Administrative Region, China (Project AoE/P-502/20), the Department of Science and Technology of Guangdong Province (2020B1515120073), and The Hong Kong Polytechnic University (1.42.XX.9B0Z).

■ REFERENCES

(1) Dixit, R.; Cyr, R. Cell damage and reactive oxygen species production induced by fluorescence microscopy: effect on mitosis and guidelines for non-invasive fluorescence microscopy. *Plant J.* **2003**, *36*, 280−290.
(2) Stemmer, A.; Beck, M.; Fiolka, R. Widefield fluorescence microscopy with extended resolution. *Histochem. Cell Biol.* **2008**, *130*, 807−817.
(3) Schermelleh, L.; Heintzmann, R.; Leonhardt, H. A guide to super-resolution fluorescence microscopy. *J. Cell Biol.* **2010**, *190*, 165−175.
(4) Gustafsson, M. G. Nonlinear structured-illumination microscopy: wide-field fluorescence imaging with theoretically unlimited resolution. *Proc. Natl. Acad. Sci. U. S. A.* **2005**, *102*, 13081−13086.
(5) Ji, N. Adaptive optical fluorescence microscopy. *Nat. Methods* **2017**, *14*, 374−380.
(6) Arbabi, E.; Li, J.; Hutchins, R. J.; Kamali, S. M.; Arbabi, A.; Horie, Y.; Van Dorpe, P.; Gradinaru, V.; Wagenaar, D. A.; Faraon, A. Two-Photon Microscopy with a Double-Wavelength Metasurface Objective Lens. *Nano Lett.* **2018**, *18*, 4943−4948.
(7) Beaulieu, D. R.; Davison, I. G.; Kilic, K.; Bifano, T. G.; Mertz, J. Simultaneous multiplane imaging with reverberation two-photon microscopy. *Nat. Methods* **2020**, *17*, 283−286.
(8) Fine, A.; Amos, W. B.; Durbin, R. M.; McNaughton, P. A. Confocal microscopy: applications in neurobiology. *Trends Neurosci.* **1988**, *11*, 346−351.
(9) Shotton, D. M. Confocal Scanning Optical Microscopy and Its Applications for Biological Specimens. *J. Cell Sci.* **1989**, *94*, 175−206.
(10) Badon, A.; Bensussen, S.; Gritton, H. J.; Awal, M. R.; Gabel, C. V.; Han, X.; Mertz, J. Video-rate large-scale imaging with Multi-Z confocal microscopy. *Optica* **2019**, *6*, 389−395.
(11) Gustafsson, M. G.; Shao, L.; Carlton, P. M.; Wang, C. J.; Golubovskaya, I. N.; Cande, W. Z.; Agard, D. A.; Sedat, J. W. Three-dimensional resolution doubling in wide-field fluorescence microscopy by structured illumination. *Biophys. J.* **2008**, *94*, 4957−4970.
(12) Karadaglic, D.; Wilson, T. Image formation in structured illumination wide-field fluorescence microscopy. *Micron* **2008**, *39*, 808−818.
(13) Lim, D.; Ford, T. N.; Chu, K. K.; Mertz, J. Optically sectioned in vivo imaging with speckle illumination HiLo microscopy. *J. Biomed. Opt.* **2011**, *16*, 016014.
(14) Schniete, J.; Franssen, A.; Dempster, J.; Bushell, T. J.; Amos, W. B.; McConnell, G. Fast Optical Sectioning for Widefield Fluorescence Mesoscopy with the Mesolens based on HiLo Microscopy. *Sci. Rep.* **2018**, *8*, 16259.
(15) Zhang, H.; Vyas, K.; Yang, G. Z. Line scanning, fiber bundle fluorescence HiLo endomicroscopy with confocal slit detection. *J. Biomed. Opt.* **2019**, *24*, 1−7.
(16) Lim, D.; Chu, K. K.; Mertz, J. Wide-field fluorescence sectioning with hybrid speckle and uniform-illumination microscopy. *Opt. Lett.* **2008**, *33*, 1819−1821.
(17) Mertz, J. Optical sectioning microscopy with planar or structured illumination. *Nat. Methods* **2011**, *8*, 811−819.
(18) Shi, R.; Jin, C.; Xie, H.; Zhang, Y.; Li, X.; Dai, Q.; Kong, L. Multi-plane, wide-field fluorescent microscopy for biodynamic imaging in vivo. *Biomed. Opt. Express* **2019**, *10*, 6625−6635.
(19) Hsiao, H.; Lin, C. Y.; Vyas, S.; Huang, K. Y.; Yeh, J. A.; Luo, Y. Telecentric design for digital-scanning-based HiLo optical sectioning endomicroscopy with an electrically tunable lens. *J. Biophotonics* **2021**, *14* (2), e202000335.
(20) Ren, H.; Wu, S. T. Variable-focus liquid lens. *Opt. Express* **2007**, *15*, 5931−5936.
(21) Ye, M.; Wang, B.; Takahashi, T.; Sato, S. Properties of variable-focus liquid crystal lens and its application in focusing system. *Opt. Rev.* **2007**, *14*, 173−175.
(22) Liebetraut, P.; Petsch, S.; Liebeskind, J.; Zappe, H. Elastomeric lenses with tunable astigmatism. *Light: Sci. Appl.* **2013**, *2*, e98.
(23) Bernet, S.; Ritsch-Marte, M. Adjustable refractive power from diffractive moiré elements. *Appl. Opt.* **2008**, *47*, 3722−3730.
(24) Burch, J. M.; Williams, D. C. Varifocal moiré zone plates for straightness measurement. *Appl. Opt.* **1977**, *16*, 2445−2450.
(25) Bawart, M.; May, M. A.; Ottl, T.; Roider, C.; Bernet, S.; Schmidt, M.; Ritsch-Marte, M.; Jesacher, A. Diffractive tunable lens for remote focusing in high-NA optical systems. *Opt. Express* **2020**, *28*, 26336−26347.
(26) Avrutsky, I.; Chaganti, K.; Salakhutdinov, I.; Auner, G. Concept of a miniature optical spectrometer using integrated optical and micro-optical components. *Appl. Opt.* **2006**, *45*, 7811−7817.
(27) Bawart, M.; Jesacher, A.; Zelger, P.; Bernet, S.; Ritsch-Marte, M. Modified Alvarez lens for high-speed focusing. *Opt. Express* **2017**, *25*, 29847−29855.
(28) Wang, S. M.; Wu, P. C.; Su, V. C.; Lai, Y. C.; Chen, M. K.; Kuo, H. Y.; Chen, B. H.; Chen, Y. H.; Huang, T. T.; Wang, J. H.; Lin, R. M.; Kuan, C. H.; Li, T.; Wang, Z. L.; Zhu, S. N.; Tsai, D. P. A broadband achromatic metalens in the visible. *Nat. Nanotechnol.* **2018**, *13*, 227−232.
(29) Wang, S.; Wu, P. C.; Su, V.-C.; Lai, Y.-C.; Hung Chu, C.; Chen, J.-W.; Lu, S.-H.; Chen, J.; Xu, B.; Kuan, C.-H.; Li, T.; Zhu, S.; Tsai, D. P. Broadband achromatic optical metasurface devices. *Nat. Commun.* **2017**, *8*, 187.
(30) Wu, P. C.; Chen, J.-W.; Yin, C.-W.; Lai, Y.-C.; Chung, T. L.; Liao, C. Y.; Chen, B. H.; Lee, K.-W.; Chuang, C.-J.; Wang, C.-M.; Tsai, D. P. Visible metasurfaces for on-chip polarimetry. *ACS Photonics* **2018**, *5*, 2568−2573.
(31) Huang, Y. W.; Chen, W. T.; Tsai, W. Y.; Wu, P. C.; Wang, C. M.; Sun, G.; Tsai, D. P. Aluminum plasmonic multicolor meta-hologram. *Nano Lett.* **2015**, *15*, 3122−3127.
(32) Faraji-Dana, M.; Arbabi, E.; Kwon, H.; Kamali, S. M.; Arbabi, A.; Bartholomew, J. G.; Faraon, A. Hyperspectral Imager with Folded Metasurface Optics. *ACS Photonics* **2019**, *6*, 2161−2167.
(33) Li, L.; Liu, Z.; Ren, X.; Wang, S.; Su, V. C.; Chen, M. K.; Chu, C. H.; Kuo, H. Y.; Liu, B.; Zang, W.; Guo, G.; Zhang, L.; Wang, Z.; Zhu, S.; Tsai, D. P. Metalens-array-based high-dimensional and multiphoton quantum source. *Science* **2020**, *368*, 1487−1490.
(34) Pahlevaninezhad, H.; Khorasaninejad, M.; Huang, Y. W.; Shi, Z.; Hariri, L. P.; Adams, D. C.; Ding, V.; Zhu, A.; Qiu, C. W.; Capasso, F.; Suter, M. J. Nano-optic endoscope for high-resolution optical coherence tomography in vivo. *Nat. Photonics* **2018**, *12*, 540−547.
(35) Zhang, S.; Wong, C. L.; Zeng, S.; Bi, R.; Tai, K.; Dholakia, K.; Olivo, M. Metasurfaces for biomedical applications: imaging and sensing from a nanophotonics perspective. *Nanophotonics* **2020**, *10*, 259−293.

https://doi.org/10.1021/acs.nanolett.1c01114
Nano Lett. 2021, 21, 5133−5142

(36) Lin, R. J.; Su, V. C.; Wang, S. M.; Chen, M. K.; Chung, T. L.; Chen, Y. H.; Kuo, H. Y.; Chen, J. W.; Chen, J.; Huang, Y. T.; Wang, J. H.; Chu, C. H.; Wu, P. C.; Li, T.; Wang, Z. L.; Zhu, S. N.; Tsai, D. P. Achromatic metalens array for full-colour light-field imaging. *Nat. Nanotechnol.* **2019**, *14*, 227−232.
(37) Chen, M. K.; Wu, Y. F.; Feng, L.; Fan, Q. B.; Lu, M. H.; Xu, T.; Tsai, D. P. Principles, Functions, and Applications of Optical Meta-Lens. *Adv. Opt. Mater.* **2021**, *9*, 2001414.
(38) Yu, N.; Genevet, P.; Kats, M. A.; Aieta, F.; Tetienne, J. P.; Capasso, F.; Gaburro, Z. Light propagation with phase discontinuities: generalized laws of reflection and refraction. *Science* **2011**, *334*, 333−337.
(39) Colburn, S.; Zhan, A.; Majumdar, A. Varifocal zoom imaging with large area focal length adjustable metalenses. *Optica* **2018**, *5*, 825−831.
(40) Colburn, S.; Majumdar, A. Simultaneous Achromatic and Varifocal Imaging with Quartic Metasurfaces in the Visible. *ACS Photonics* **2020**, *7*, 120−127.
(41) Arbabi, E.; Arbabi, A.; Kamali, S. M.; Horie, Y.; Faraji-Dana, M.; Faraon, A. MEMS-tunable dielectric metasurface lens. *Nat. Commun.* **2018**, *9*, 812.
(42) Wei, Y.; Wang, Y.; Feng, X.; Xiao, S.; Wang, Z.; Hu, T.; Hu, M.; Song, J.; Wegener, M.; Zhao, M.; Xia, J.; Yang, Z. Compact Optical Polarization-Insensitive Zoom Metalens Doublet. *Adv. Opt. Mater.* **2020**, *8*, 2000142.
(43) Guo, Y.; Pu, M.; Ma, X.; Li, X.; Shi, R.; Luo, X. Experimental demonstration of a continuous varifocal metalens with large zoom range and high imaging resolution. *Appl. Phys. Lett.* **2019**, *115*, 163103.
(44) Ee, H. S.; Agarwal, R. Tunable Metasurface and Flat Optical Zoom Lens on a Stretchable Substrate. *Nano Lett.* **2016**, *16*, 2818−2823.
(45) Barker, A. S.; Ilegems, M. Infrared Lattice-Vibrations and Free-Electron Dispersion in Gan. *Phys. Rev. B* **1973**, *7*, 743−750.
(46) Su, V. C.; Chu, C. H.; Sun, G.; Tsai, D. P. Advances in optical metasurfaces: fabrication and applications [Invited]. *Opt. Express* **2018**, *26*, 13148−13182.
(47) Bernet, S.; Harm, W.; Ritsch-Marte, M. Demonstration of focus-tunable diffractive Moiré-lenses. *Opt. Express* **2013**, *21*, 6955−6966.
(48) Kim, J. S.; Kanade, T. Multiaperture telecentric lens for 3D reconstruction. *Opt. Lett.* **2011**, *36*, 1050−1052.
(49) Lin, C. Y.; Lin, W. H.; Chien, J. H.; Tsai, J. C.; Luo, Y. In vivo volumetric fluorescence sectioning microscopy with mechanical-scan-free hybrid illumination imaging. *Biomed. Opt. Express* **2016**, *7*, 3968−3978.
(50) Pendharker, S.; Shende, S.; Newman, W.; Ogg, S.; Nazemifard, N.; Jacob, Z. Axial super-resolution evanescent wave tomography. *Opt. Lett.* **2016**, *41*, 5499−5502.

https://doi.org/10.1021/acs.nanolett.1c01114
Nano Lett. 2021, 21, 5133−5142